Journal of
Clinical Medicine

MDPI

Article

Influence of Cross-Section and Pitch on the Mechanical Response of NiTi Endodontic Files under Bending and Torsional Conditions—A Finite Element Analysis

Victor Roda-Casanova [1], Antonio Pérez-González [1], Alvaro Zubizarreta-Macho [2,3,*] and Vicente Faus-Matoses [4]

[1] Department of Mechanical Engineering and Construction, Universitat Jaume I, 12071 Castelló de la Plana, Spain; vroda@uji.es (V.R.-C.); aperez@uji.es (A.P.-G.)
[2] Department of Dentistry, Alfonso X el Sabio University, 28691 Madrid, Spain
[3] Department of Orthodontics, University of Salamanca, 37008 Salamanca, Spain
[4] Department of Stomatology, Faculty of Medicine and Dentistry, University of Valencia, 46010 Valencia, Spain; vfaus@clinicafaus.com
* Correspondence: amacho@uax.es

Abstract: In this article, the effects of cross-section and pitch on the mechanical response of NiTi endodontic files is studied by means of finite element analyses. The study was conducted over a set of eight endodontic rotary files, whose geometry was obtained from combinations of two cross-sections (square and triangular) and four pitches. Each file was subjected to bending and torsional analyses, simulating the testing conditions indicated in the ISO 3630 Standard, in order to assess their stiffness and mechanical strength. The results indicate that endodontic files with a square cross-section have double the stiffness of those with triangular cross-sections, both in terms of bending and torsion. For both loading modes, endodontic files with a triangular cross-section can undergo larger deformations before overload failure than those with a square cross-section: up to 20% more in bending and 40% in torsion. Moreover, under equivalent boundary conditions, endodontic files with triangular cross-sections present a higher fatigue life than those with square cross-sections: up to more than 300% higher for small pitches. The effect of pitch on the stiffness and strength of the file is smaller than that of the cross-section shape, but smaller pitches could be beneficial when using a triangular cross-section, as they increase the bending flexibility, fatigue life, and torsion stiffness. These results suggest a clinical recommendation for the use of files with a triangular-shaped cross-section and a small pitch in order to minimize ledging and maximize fatigue life. Finally, in this study, we reveal the sensitivity of the orientation of files with respect to the bending direction, which must be taken into account when designing, reporting, and interpreting test results under such loading conditions.

Keywords: endodontic file; cross-section; pitch; flexural bending; torsion; stress distribution; finite element analysis

Citation: Roda-Casanova, V.; Pérez-González, A.; Zubizarreta-Macho, A.; Faus-Matoses, V. Influence of Cross-Section and Pitch on the Mechanical Response of NiTi Endodontic Files under Bending and Torsional Conditions—A Finite Element Analysis. *J. Clin. Med.* **2022**, *11*, 2642. https://doi.org/10.3390/jcm11092642

Academic Editors: Massimo Amato, Giuseppe Pantaleo and Alfredo Iandolo

Received: 18 April 2022
Accepted: 5 May 2022
Published: 8 May 2022

1. Introduction

The introduction of nickel–titanium alloy (NiTi) for the manufacturing of root canal instruments entailed a great revolution in the field of endodontics, as the consequent endodontic files decreased the incidence of iatrogenic complications [1,2]. However, despite the continuous mechanical and chemical improvements made by manufacturers, the failure of endodontic files during root canal treatments remains a concern for clinicians [3], as the incidence of their fracture still ranges from 0.09% to 5% [4,5].

The fracture of rotary instruments occurs mainly due to two different mechanisms, usually referred to as torsion overload and flexural fatigue [6,7]. On one hand, the torsion overload failure mechanism corresponds to a static failure that typically occurs when the tip of the endodontic file becomes blocked in the root canal whilst the instrument continues

rotating [8]. In static failure, the file fails because the stress value reaches the elastic limit of the material, such that the file undergoes permanent deformation and finally fractures. On the other hand, flexural fatigue is a failure mechanism produced mainly by the alternating compressive and tensile stresses and strains that appear in any point of a file rotating inside a curved root canal [8,9]. This type of fatigue failure results in a sudden fracture of the file after a certain number of rotations, even if the stress levels are far below the elastic limit of the material, due to the nucleation and progression of small cracks in some stressed sections of the file. Thus, bending and torsion are essential conditions to evaluate the mechanical behavior of endodontic instruments [10]. The unexpected failure of NiTi endodontic files may condition the outcome of the root canal treatment by blocking the advancement of disinfecting agents beyond the fractured instrument [11–13], which may lead to subsequent pulp necrosis and the formation of periapical lesions [14], or decrease the success rate of root canal treatment of teeth with periapical pathology [15]. In addition, extraction of the fractured NiTi endodontic rotary file from the root canal system requires root dentin removal to provide access to the fractured instruments [16]. This causes a loss of dentin tissue, which can negatively affect the structural integrity of the tooth [17]. Furthermore, it can lead to root perforation and increase the risk of vertical root fracture, especially in the apical third [16]. For these reasons, a better understanding of the independent and combined effects of the different parameters that affect these failure mechanisms is desirable, and additional research must be addressed to this end.

Several works have been conducted to analyze the influence of both the NiTi alloy [18] and the geometrical parameters on the torsional and bending resistance of endodontic instruments. Both the chemical composition and crystalline structure of the NiTi alloy have been studied, and it has been shown that they highly influence the strength of the endodontic file [19]. In particular, endodontic rotary systems with a higher concentration of the martensitic phase and manufactured using electropolishing, ion implantation, cryogenic treatment, and heat treatments improve the mechanical behavior of NiTi endodontic rotary files, increasing their cyclic fatigue resistance. The geometric parameters of the endodontic files have also been reported to influence the instrument's performance, including the taper and apical diameter [20], cross-section design [21,22], flute length, helix angle, and pitch [23]. The influence of these variables has been analyzed using static and dynamic custom-made cyclic fatigue testing devices, which have not been submitted to a standardization normative, and do not allow for independently assessing the influence of each geometric parameter associated with flexural fatigue or torsional overload. There are other standardized testing devices, such as those described in ISO 3630-1:2008 [24], which allow for the independent assessment of both torsional and bending phenomena, although their capability to reproduce the actual operating conditions of endodontic files has not yet been verified.

Computer simulation has proven to be an interesting tool for studying the failure of endodontic rotary files. In the simplest cases, analytical methods can be used for such a purpose, which are usually based on the small strain theory of elasticity. In this line, Zhang et al. [25] have analyzed the mechanical behavior of NiTi endodontic files under torsional and bending loads. Tsao et al. [26] have developed analytical models to study the flexibility of NiTi instruments subjected to bending loads. These analytical models have the advantage of being fast and easy to implement, but their capabilities to consider non-linear behaviors (i.e., material non-linearity) or complex loading scenarios are limited. These limitations can be overcome by using numerical methods such as the finite element method.

The ability of the finite element method to reproduce the results obtained from experimental tests using endodontic rotary files has been proven in several works [7,10,27–29], whose main conclusions have been summarized in a recent bibliographical review [30]. This review concluded that the finite element method is a reliable tool for evaluating the behavior of NiTi rotary instruments, and has the advantage of reducing instrument development time and costs. Another important advantage of the finite element method is that it also allows us to assess aspects of the mechanical behavior of the instruments, such as the

stress distribution, which are difficult to obtain in laboratory tests [10]. The finite element method has been previously used to analyze the influence of cross-section design and pitch on the stiffness and stress distribution under bending and torsional conditions [10,31–37]. Appendix B collects detailed information about these previous studies, including their main conclusions and limitations. Some of these studies have used proprietary file models, such as ProTaper, ProFile, Mtwo, and others, which hampers the independent evaluation of parameters such as cross-section geometry, cross-section area, or pitch [10,32–35]. Other studies have used theoretical file models to avoid this problem, but with some limitations; for example, in [36], the authors analyzed four different cross-sections and three pitch values under torsion, but did not provide detailed information about the material model for the shape memory alloy (SMA) of the files or about the quality of the finite element mesh. In another study, Versluis et al. [33] analyzed the effects of pitch and cross-section geometry on flexural stiffness and stresses using a representative SMA material model. However, the boundary conditions were specified differently to those in ISO 3630-1:2008 [24] and the bending applied was low, leading to maximum von Mises stresses below the initial stress for transformation from austenite to martensite, and, thus, the effect of the super-elasticity of the files was not analyzed; furthermore, torsion behavior was not included in the study. In [37], the effect of cross-section geometry and pitch on the 'screw-in' tendency of the files was analyzed, but a linear material model was used for the file. A more recent study investigated different geometric options for the sides of a triangle-shaped cross-section (straight, convex, and concave), as well as the use of files with combinations of these geometries along the file [31], but the pitch effect was not analyzed.

Some of these finite element models are limited in their accuracy, in terms of representing the correct geometry and boundary conditions of the endodontic files, or use simplified material models that are incapable of representing their actual mechanical response under load. In this study, we address all of these partial limitations of previous studies by undertaking a comprehensive analysis of the effects of pitch and cross-section using an accurate finite element model that allows us to simulate the testing conditions of the ISO3630 Standard to the best extent possible. The method used to obtain the parametric geometrical representation of the endodontic instrument and the corresponding finite element mesh has been proposed in our previous work [38]. The use of an accurate numerical model in these tests can foster improvements in new generations of more resistant and flexible endodontic files, reducing the need for expensive and time-consuming experiments in the early design stages. From a clinical perspective, these improvements are expected to reduce the risk of failure of endodontic instruments, thus preventing clinical complications.

The aim of this study was to analyze and compare the effects of the cross-section and the pitch on the mechanical response (in terms of strength and stiffness) of NiTi endodontic files under bending and torsional conditions, similar to those indicated in the ISO 3630 Standard [24], using the finite element method. The study was conducted using a set of eight different endodontic rotary files whose geometries were obtained from combinations of two cross-sections (triangular and square) and four pitches (1 mm, 2 mm, 4 mm, and 8 mm). Under these conditions, the following individual objectives were pursued: (i) to develop a finite element model which reproduces the experimental tests conducted in the ISO 3630 Standard; (ii) to conduct a bending analysis of the selected endodontic rotary files, in order to predict the stiffness and strength of the files under static and cyclic loading conditions; and (iii) to conduct a torsional analysis of the selected endodontic rotary files, in order to predict the stiffness and the strength of the files under static loading conditions.

2. Materials and Methods

For this study, different endodontic instruments were analyzed using numerical simulation with finite elements. Figure 1 shows the geometries of the eight endodontic files considered. The different geometries were obtained by varying the cross-section (square and triangular) and the pitch ($p_z = \{1\text{ mm}, 2\text{ mm}, 4\text{ mm}, 8\text{ mm}\}$) of the files. All of them had a total length of $L_{total} = 25$ mm, the length of their active part was $L_a = 16$ mm, and

their tip and shaft diameters were $d_a = 0.25$ mm and $d_{sh} = 1.20$ mm, respectively. The taper of the endodontic files was 6%.

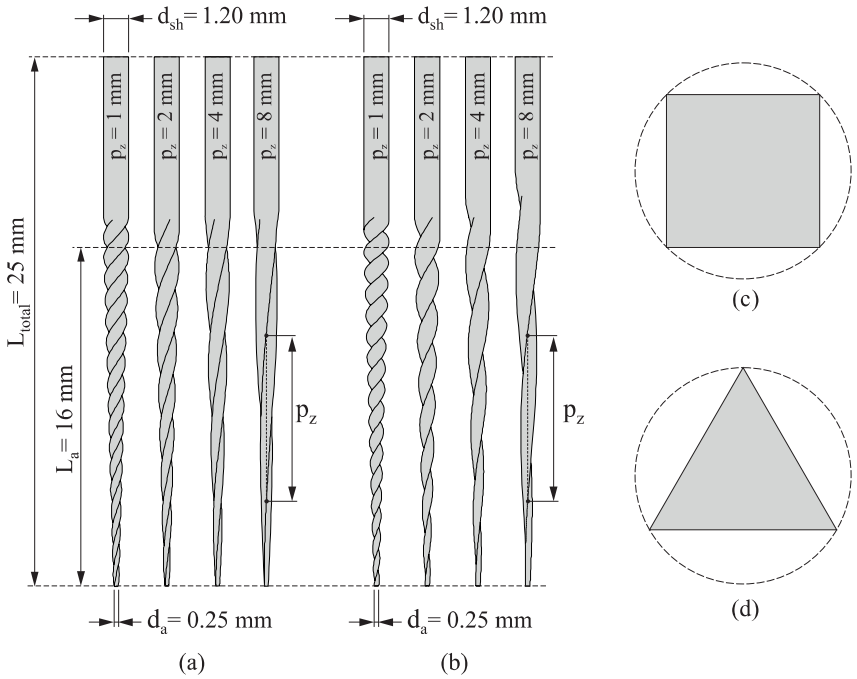

Figure 1. Geometries of the analyzed endodontic files: endodontic files with square cross-section (**a**); endodontic files with triangular cross-section (**b**); normalized square cross-section (**c**); and normalized triangular cross-section (**d**).

The material for all the files was considered to be NiTi, which exhibits a super-elastic stress–strain curve, as shown in Figure 2. Here, E_A and E_M represent the Young's moduli of austenite and martensite, respectively. The beginning and end of the loading phase transformation are denoted by σ_L^S and σ_L^E, respectively, whereas the beginning and the end of the unloading transformation phase are denoted by σ_U^S and σ_U^E. Finally, ε_L represents the uni-axial transformation strain, and σ_{ME}^E indicates the end of the martensitic elastic regime.

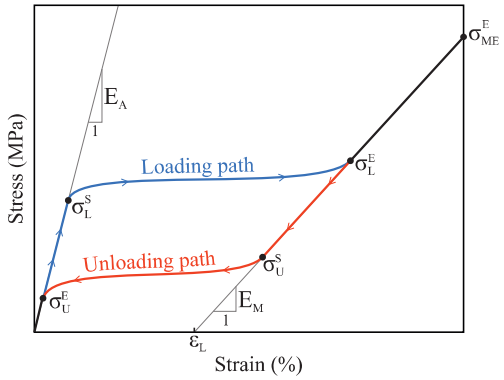

Figure 2. Sample stress–strain curve for NiTi material.

2.1. Devices for Experimental Bending and Torsion Analysis

Endodontic files are usually tested in terms of bending and torsional loads, and the typical standardized procedure for these tests has been described in the ISO 3630 Standard [24], as summarized in Figure 3. For the torsion analysis (Figure 3a), the last 3 mm at the tip of the endodontic file are inserted inside a clamping jaw. After checking that the endodontic file is properly fixed and aligned with the axis of rotation, the top of the file is rigidly connected to the torsion device. This torsion device is increasingly rotated

at angle θ_z, and the torsional moment M_z is measured using a torquemeter attached to the clamping jaw. The test ends with the failure of the endodontic file. At this point, the maximum rotated angle $\theta_{z,max}$ and maximum torsional moment $M_{z,max}$ are registered.

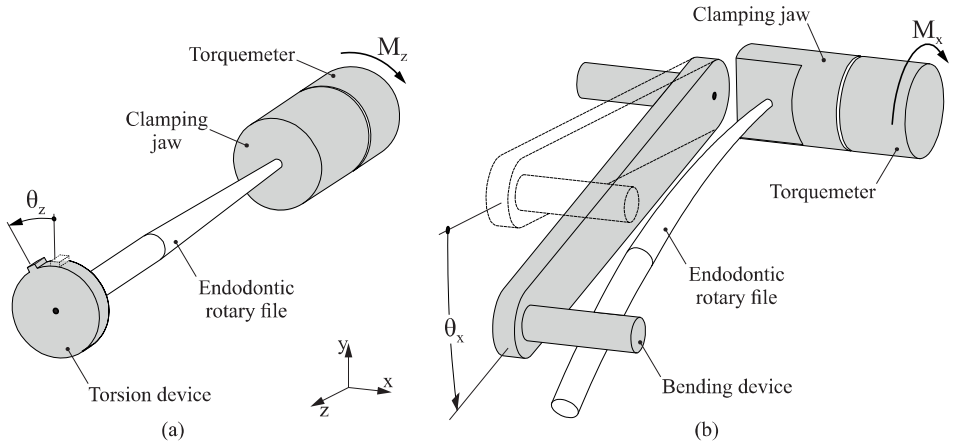

Figure 3. Devices used for torsion (**a**) and bending (**b**) analyses.

In a similar way, in the bending analysis (Figure 3b), the last 3 mm at the tip of the endodontic file are inserted inside a clamping jaw. After checking that the endodontic file is properly fixed and aligned with the axis of rotation, the bending device is positioned until it contacts the endodontic file. Then, the bending device is increasingly rotated at angle θ_x, and the bending moment M_x is measured using a torquemeter attached to the clamping jaw. The test ends with the failure of the endodontic file. At this point, the maximum rotated angle $\theta_{x,max}$ and maximum bending moment $M_{x,max}$ are registered.

2.2. Definition of the Finite Element Model for the NiTi Endodontic File

Figure 4 shows an example of the finite element model created for the endodontic file simulation experiments, as described in Section 2.1. Here, only the portion of the endodontic file subjected to stresses and strains was considered in the analysis (i.e., the part of the endodontic file inserted into the clamping jaw was not included in the finite element model). The geometry of the endodontic file was generated and then discretized into quadratic finite element tetrahedrons following the meshing procedure developed in our previous work [38]. Using this procedure, the finite element mesh of a endodontic file was automatically built from its geometrical parameters (d_{sh}, d_a, L_a, L_{total}, and p_z, as shown in Figure 1) and the average element size.

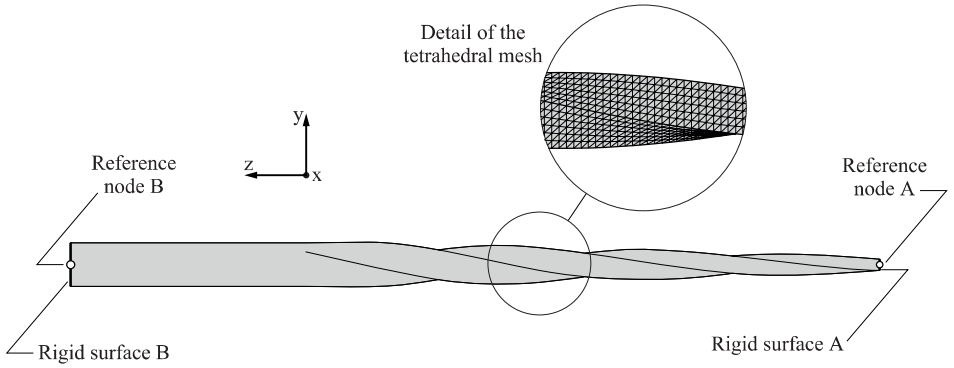

Figure 4. Definition of the finite element model.

To select the average element size, a mesh sensitivity study was conducted in our previous work [38] for a finite element model of an endodontic file with similar geometry, element type, boundary, and loading conditions, as described in Figure 4. In this study, the variations in the maximum element energy error and energy norm error with respect to the

average element size were observed, and it was concluded that an average element size equal to 0.1 mm provided a good compromise between accuracy and computational cost. For these reasons, this average element size was used to perform this study, resulting in a finite element model with 89,295 nodes and 58,749 elements.

The super-elastic behavior of the NiTi alloy used to manufacture the endodontic files was modeled using the material model developed by Auricchio [39]. The material properties that characterize this material model were extracted from [10], and are shown in Table 1.

Table 1. Material properties to characterize the super-elastic behavior of NiTi alloy. Reprinted/adapted with permission from Ref. [10]. 2014, Elsevier.

Parameter	Variable	Magnitude
Young's modulus of austenite	E_A	42,530 MPa
Austenite Poisson's ratio	ν_A	0.33
Young's modulus of martensite	E_M	12,828 MPa
Martensite Poisson's ratio	ν_M	0.33
Uni-axial transformation strain	ε_L	6%
Slope of the stress–temperature curve for loading	$(\delta\sigma/\delta T)_L$	6.7
Start of transformation loading	σ_L^S	492 MPa
End of transformation loading	σ_L^E	630 MPa
Reference temperature	T_0	22 °C
Slope of the stress–temperature curve for unloading	$(\delta\sigma/\delta T)_U$	6.7
Start of transformation unloading	σ_U^S	192 MPa
End of transformation unloading	σ_U^E	97 MPa
End of martensitic elastic regime	σ_{ME}^E	1200 MPa

The surface at the fixed end of the endodontic file was defined as a rigid surface (denoted as rigid surface A in Figure 4). This rigid surface was rigidly connected to reference node A, which was used to introduce the boundary conditions for the finite element model. To simulate the effect of the clamping jaw over the endodontic file, all of the degrees of freedom of reference node A were restricted. At the other side of the file, the top surface was also defined as a rigid surface (denoted as rigid surface B in Figure 4). This rigid surface was rigidly connected to reference node B, which was used to define the loading conditions of the model. Two different loading conditions were considered in the analyses, one for the bending analysis and the other for the torsional analysis:

- In the bending analysis, an increasing displacement was imposed at reference node B in the negative direction of the y-axis, until the maximum von Mises stress along the endodontic file σ_{max} reached the end of the martensitic elastic regime. As the results of the bending analyses are sensitive to the orientation of the endodontic file with respect to the bending direction, the analysis was conducted in 24 different angular positions, given by a rotation $\varphi_z = \{0°, 15°, 30°, \ldots, 360°\}$ of the endodontic file with respect to the z-axis.
- In the torsional analysis, an increasing rotation was imposed at reference node B along the positive direction of z-axis, until the maximum von Mises stress along the endodontic file σ_{max} reached the end of the martensitic elastic regime. Here, the results of the analysis do not depend on the orientation of the file.

The finite element model was solved through transient analysis using the large displacements formulation, which was conducted using the ABAQUS software. Hence, material and geometric non-linearities were considered in the study. In each one of these analyses, the rotation at reference node B (θ_x for bending analysis and θ_z for torsional analysis) and the reaction moment at reference node A (M_x for bending analysis and M_z for torsional analysis) were registered for each analysis frame. The maximum von Mises stress and the maximum principal strain were also retrieved for each analysis frame, using the

method indicated in Appendix A.1, in order to minimize possible numerical singularities in the model. Finally, the bending fatigue life was estimated following the method described in Appendix A.2, based on the Coffin–Manson relation, considering the material properties indicated in Table 2.

Table 2. Material properties used to characterize the fatigue behavior of NiTi alloy [28,40].

Parameter	Variable	Magnitude
Fatigue ductility coefficient	$\varepsilon_F^{'}$	0.68
Fatigue strength coefficient	$\sigma_F^{'}$	705 MPa
Fatigue ductility exponent	c	−0.6
Fatigue strength exponent	b	−0.06
Modulus of elasticity	E	42.5 GPa

3. Results

3.1. Bending Analysis

Figure 5 shows the von Mises stress plot for the bending analysis of two representative endodontic files with pitch $p_z = 4$ mm and analysis angular position given by $\varphi_z = 0°$, for the analysis frame in which the maximum von Mises stress in the model reaches the end of the loading transformation phase ($\sigma_{max} = \sigma_L^E$). Figure 5a shows the von Misses stress plot over an endodontic file with square cross-section and Figure 5b shows the von Misses stress plot over an endodontic file with triangular cross-section. The figure shows that, under these boundary conditions, the highest stresses were located in the apical third of the file.

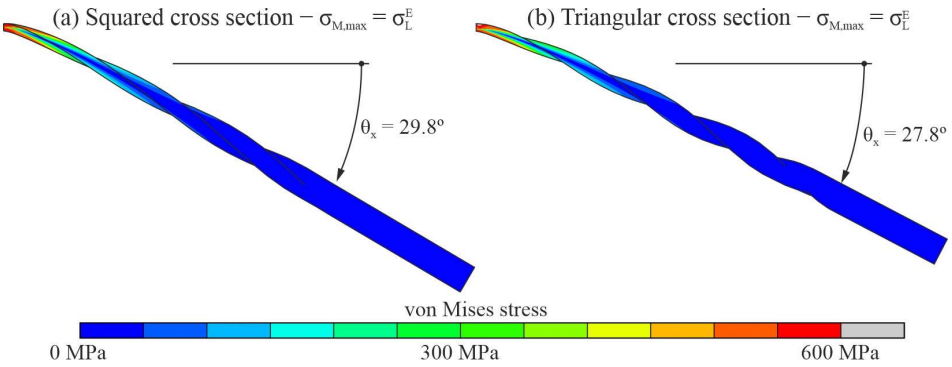

Figure 5. The von Mises stress plots for the bending analysis of endodontic files with $p_z = 4$ mm and $\varphi = 0°$.

Figure 6 shows the relationship between the rotation θ_x and the reaction bending moment M_x obtained from the bending analysis of the endodontic files with square (Figure 6a) and triangular (Figure 6b) cross-sections and pitch $p_z = 4$ mm. Here, the abscissa axis shows the rotation of the reference node B along the x-axis, while the ordinate axis shows the reaction bending moment at reference node A. The figure also shows the points where the maximum von Mises stress in the finite element model reaches the start of the phase transformation, the end of the phase transformation, and the end of the martensitic elastic regime. The curves in the figure exhibit a significant decrease in the slope for a rotation close to 20°, corresponding to a change in the stiffness of the file, as the transformation from austenite to martensite progresses in part of the file. As the bending response of an endodontic file is dependent on its orientation (given by the angle φ_z), different curves were obtained for each cross-section. For clarity, only the lower and upper curves are shown for each case, along with another intermediate representative curve. The figures also show the cross-section orientation at the encastré for each case.

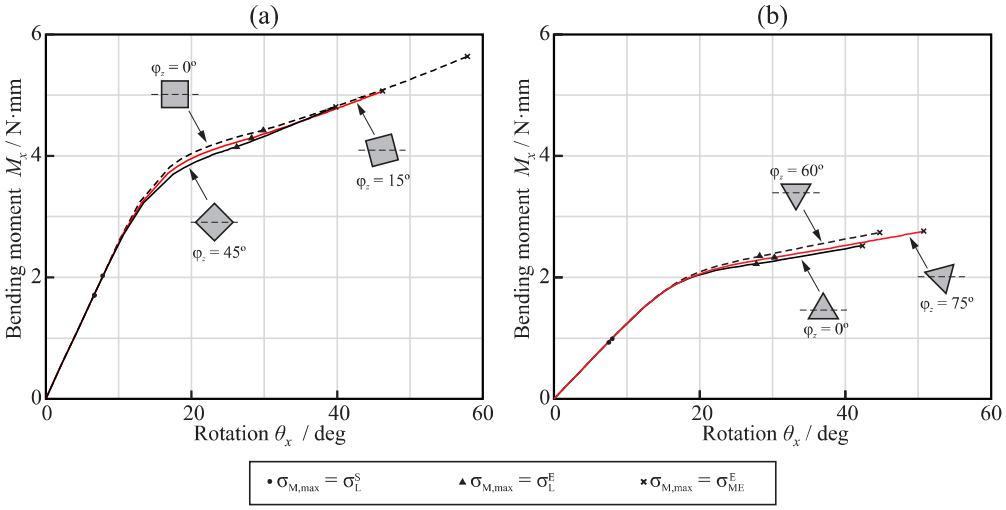

Figure 6. Bending moment–rotation relationships for the bending analysis of endodontic files with $p_z = 4$ mm: squared cross-section (**a**) and triangular cross-section (**b**).

Figure 7 shows the bending overload failure mechanism evaluation, which occurs when the maximum von Mises stress in the endodontic file reaches the end of the martensitic elastic regime ($\sigma_{max} = \sigma^E_{ME}$). On one hand, Figure 7a shows, for each considered pitch and cross-section, the rotation that needs to be applied at the free end of the endodontic files to reach the end of the martensitic elastic regime in the bending analysis. On the other hand, Figure 7b shows, for each considered pitch and cross-section, the maximum bending moment that can be applied at the free end of the endodontic files before they reach the end of the martensitic elastic regime in the bending analysis. As different angular positions were evaluated for each cross-section and pitch, the results shown are the range between the minimum and maximum obtained values. The bold lines represent the mean value within this range.

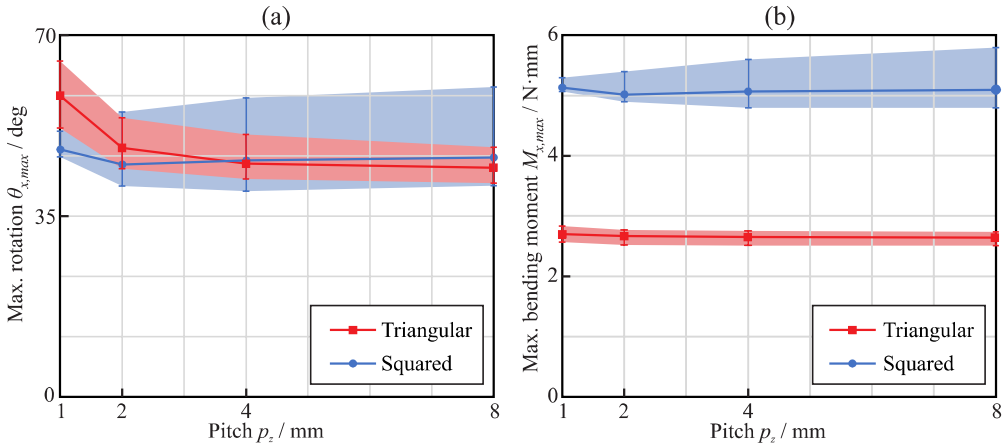

Figure 7. Bending analysis: effect of the pitch on the maximum rotation (**a**) and maximum applied torque (**b**) when the end of the martensitic elastic regime is reached.

Figure 7a shows that the maximum rotation was, on average, quite similar for triangular and square cross-sections when the pitch value was larger than 3 mm. For these pitch values, it was nearly independent of the pitch, but with a slight tendency to increase with the pitch when using a square cross-section and to decrease when using a triangular cross-section. For pitches below 3 mm, files with triangular cross-sections exhibited larger rotations than files with square cross-sections. From Figure 7b, it can be observed that the moment required to bend the square cross-section to failure was almost twice that for the triangular cross-section. The results shown in Figure 7a,b indicate that square cross-sections

are more sensitive to the orientation of the file (φ_z) than triangular cross-sections, as the results exhibited larger variability.

Figure 8 shows the bending stiffness of the endodontic rotary files for the austenite and transformation phases. The stiffness in the austenite phase was calculated as the slope of the bending moment–rotation curve before σ_L^S, while that in the transformation phase was calculated as the slope of the bending moment–rotation curve between σ_L^E and σ_{ME}^E. In general, it was observed that the stiffness of the endodontic files with square cross-sections was larger than that of the files with triangular cross-sections, both in the austenite and transformation phases. Moreover, the sensitivity to the orientation of the files with square cross-sections was larger than that of those with triangular cross-sections, especially in the austenite phase. The effect of the pitch on the stiffness was negligible for pitches larger than 3 mm. With smaller pitches, a reduction in the stiffness was observed, except for the austenite phase with the square cross-section.

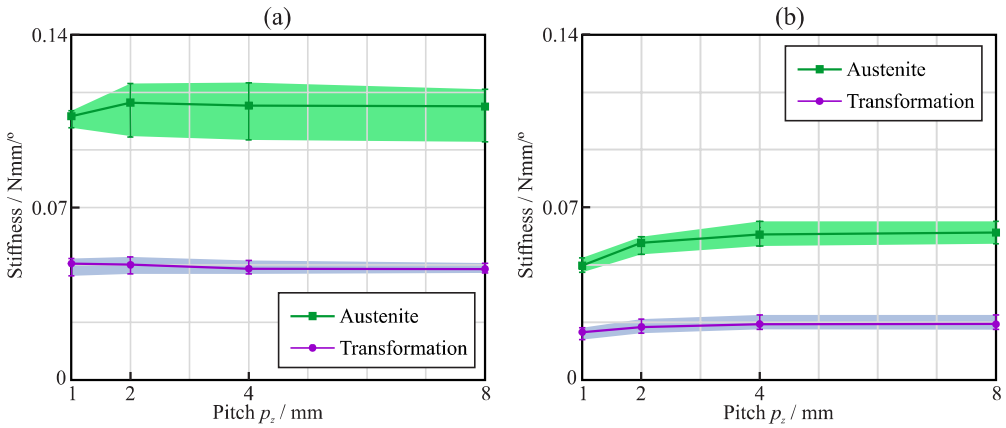

Figure 8. Bending analysis: bending stiffness of the endodontic rotary files with (**a**) square and (**b**) triangular cross-section.

Finally, Figure 9 shows the evaluation of the expected fatigue life of the endodontic files when cyclically subjected to a purely reversed bending, which produced a rotation of $\theta_x = 20°$ at the free end of the file. As explained in Appendix A.2, the bending fatigue life depends on the maximum principal strain in the file. Figure 9a shows the maximum principal strain predicted by the finite element model as a function of the pitch, for both square and triangular cross-sections. In both cases, the effect of file orientation with respect to the bending moment was significant, and the effect of the pitch was noted especially for pitches smaller than near 3 mm, for which a decrease in the strain was observed. For the square cross-section, the increase was almost linear; meanwhile, for the triangular cross-section, this increase approximated a logarithmic function. Figure 9b shows the number of cycles that the endodontic files could bear before bending fatigue failure, calculated from the maximum principal strains using the Coffin–Manson relation. It was observed that endodontic files with triangular cross-sections can withstand a larger number of cycles than those with square cross-sections, especially for small pitches.

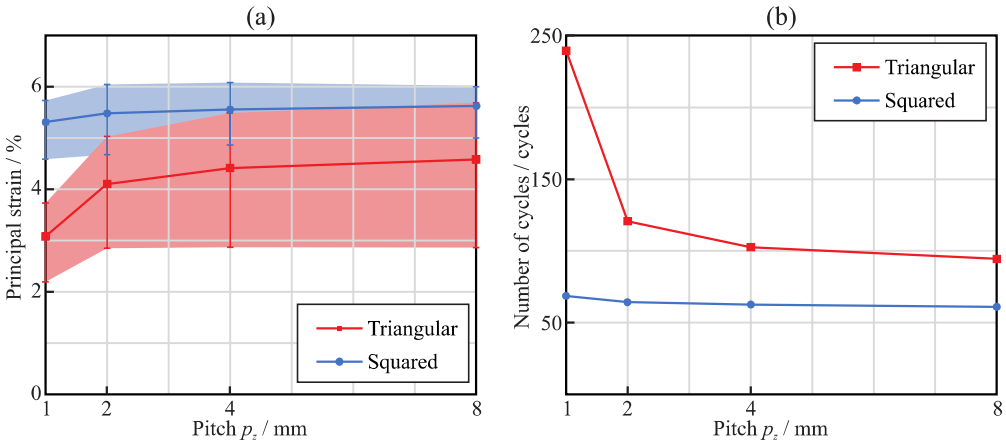

Figure 9. Bending analysis: effect of the pitch on the maximum principal strain (**a**) and the expected number of cycles (**b**) when the rotated angle is $\theta_x = 20°$.

3.2. Torsional Analysis

Figure 10 shows the von Mises stress plot for the torsional analysis of the endodontic files with square (Figure 10a) and triangular (Figure 10b) cross-sections and pitch $p_z = 4$ mm, for the analysis frames in which the maximum von Mises stress in the model reached the end of the loading transformation phase ($\sigma_{max} = \sigma_L^E$). As in the case of the bending analysis, the highest stresses were located near the apical part of the file.

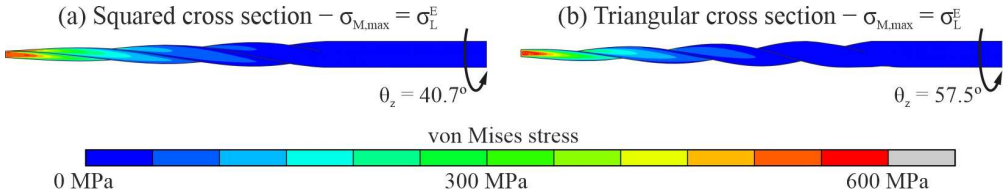

Figure 10. The von Mises stress plots for the torsional analysis of endodontic files with $p_z = 4$ mm.

Figure 11 shows the relationship between the rotation θ_z and the reaction torque M_z, obtained from the torsional analysis of the endodontic files with square (Figure 11a) and triangular (Figure 11b) cross-sections. Here, the abscissa axis shows the rotation of reference node B along the z-axis, while the ordinate axis shows the reaction torsional moment measured at reference node A. The figure also shows the points where the maximum von Mises stress in the finite element model reaches the start of the phase transformation, the end of the phase transformation, and the end of the martensitic elastic regime.

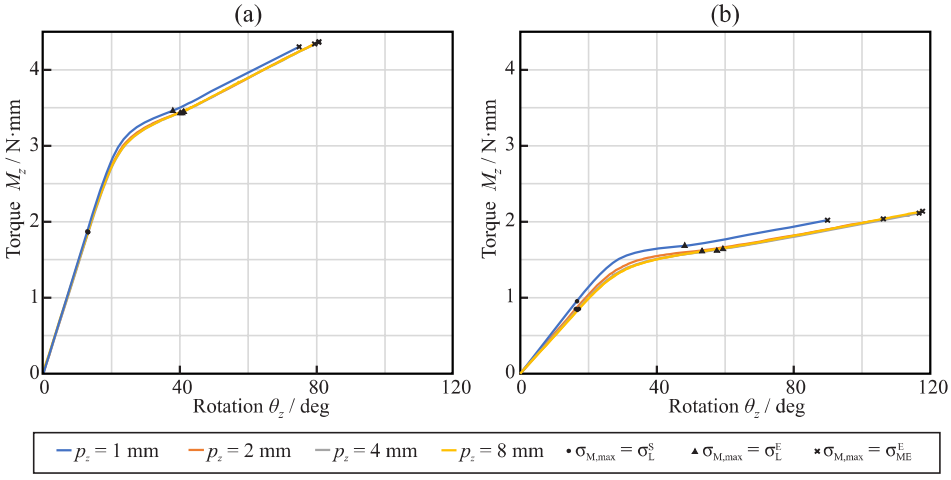

Figure 11. Torque–rotation relationships for the torsional analysis of endodontic files with different axial pitch: squared cross-section (**a**) and triangular cross-section (**b**).

Figure 12a shows, for each considered pitch and cross-section, the maximum rotation that needed to be applied at the free end of the endodontic files so that they reached the end of the martensitic elastic regime in the torsional analysis. The results show that the triangular cross-section was able to bear larger rotations before plastic deformation than the square cross-section. The rotation before failure was nearly independent of the pitch with the square cross-section, whereas it increased with the pitch for the triangular cross-section and pitch values between 1 mm and 4 mm. Figure 12b shows, for each considered pitch and cross-section, the maximum torque that could be applied at the free end of endodontic files before they reached the end of the martensitic elastic regime in the torsional analysis. It was observed that a square cross-section was able to bear almost double the torsional moment of the triangular cross-section. The strength of the files was independent of the pitch for these loading conditions.

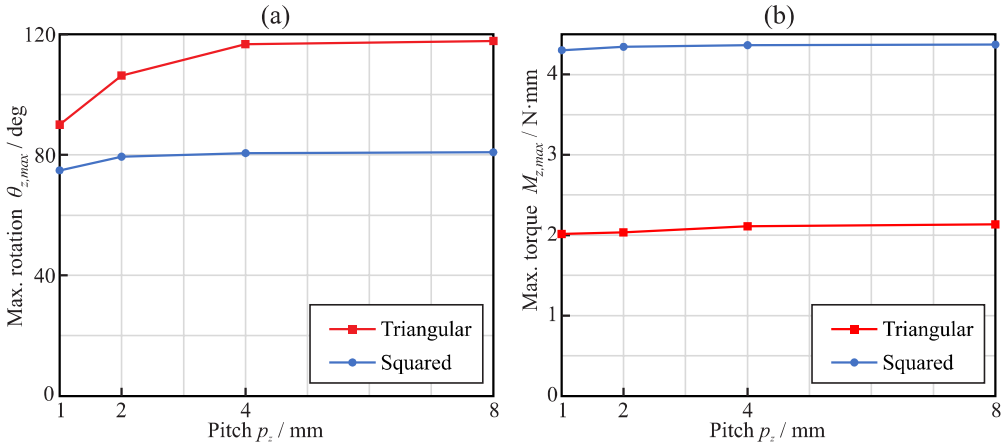

Figure 12. Torsional analysis: effect of the pitch on the applied torque (**a**) and rotation (**b**) when the end of the martensitic elastic regime is reached.

Finally, Figure 13 shows the torsional stiffness of the endodontic rotary files for the austenite and transformation phases. The stiffness in the austenite phase was calculated as the slope of the torque–rotation curve before σ_L^S, while the stiffness in the transformation phase was calculated as the slope of the torque–rotation curve between σ_L^E and σ_{ME}^E. In general, it was observed that the stiffness of the endodontic files with a square cross-section was larger than that of those with a triangular cross-section, both in the austenite and transformation phases.

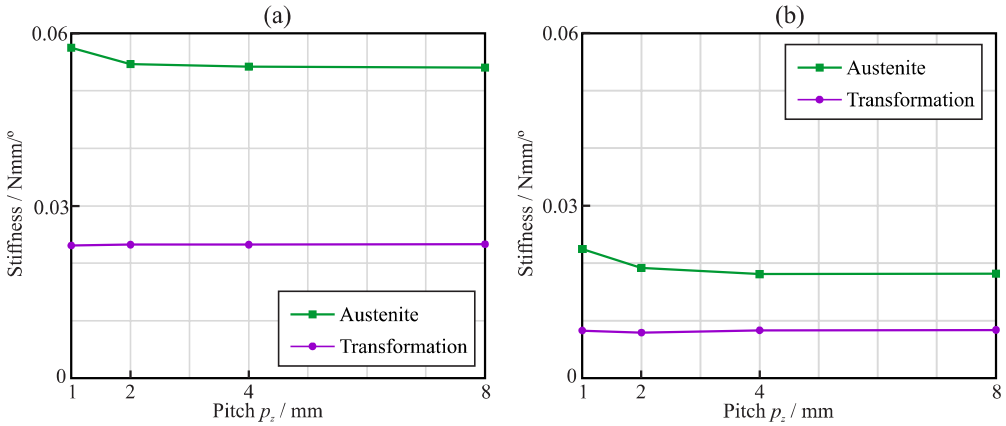

Figure 13. Torsional analysis: torsion stiffness of the endodontic rotary files with (**a**) square and (**b**) triangular cross-section.

4. Discussion

In this study, we applied an accurate non-linear finite element model to better understand the effects of the cross-section and pitch of NiTi endodontic files on their mechanical response under bending and torsion loads, according to the ISO 3630 Standard. Finite element analysis has been shown to be a good tool for this type of analysis, providing information about the stress distribution and circumventing experimental variability limitations [24]. Previous research using simulation with the same or similar objectives was first thoroughly analyzed, and the main conclusions and limitations of these studies are summarized in Appendix B, as a reference for further research. The importance of this research is supported by fact that the failure of endodontic files during root canal treatments remains a serious concern for clinicians.

The results of this study demonstrated that, for equal file diameter and taper, the cross-section shape, either triangular or square, has a greater effect than the pitch on the flexural and torsional stiffness of the file. The use of a square cross-section more than doubled the stiffness, compared to that of the triangular cross-section, as explained by the greater second moment of the area of the cross-section. The effect of pitch on stiffness was only appreciable for pitches lower than 3 mm, and was more important for triangular than for square cross-sections. When a NiTi file is bent or twisted, according to the conditions of ISO 3630, the super-elastic behavior of the material appears—which is evident from a significant decrease in the stiffness of the file—as a result of the progression of the transformation from the austenite to martensite phase in the most stressed areas of the file (see Figures 6 and 11). Our results indicate that, for a file with a shaft diameter of 1.2 mm and 6% taper, this change in stiffness appears when the rotation of the shank end section, with respect to the tip end section, is approximately 20° in bending or 30° in torsion. The stiffness of the file decreases by a factor greater than 2 after this transformation point (Figures 8 and 13). The file pitch has the opposite effect on the stiffness for torsion and bending: decreasing the pitch reduces the flexural stiffness, but increases the torsional stiffness. This effect is common for triangular and square cross-sections in the austenite phase, but it is less clear in the transformation phase, where the stiffness is less affected by pitch. This result is in agreement with those obtained in [33,36] for bending and torsion, respectively. As indicated in [33], pitch reduction could benefit both cutting efficiency, due to the higher torsional stiffness, and better adaptation to the canal shape, due to lower bending stiffness.

The obtained stress distributions (Figures 5 and 10) indicate that, for the boundary conditions imposed by the ISO 3630 Standard, the highest stresses were located near the tip of the file (where it is clamped), both in terms of bending and torsion and for both cross-section shapes. The stresses in the proximal part of the file were negligible when the stress corresponding to the end of the loading transformation phase ($\sigma_{max} = \sigma_L^E$) was reached in the tip of the file. This can be explained by the smaller section at the tip and, in the case of bending, by the higher bending moment in this area.

Static failure under bending was obtained for comparable rotations—close to 40° for pitch greater than 3 mm and ranging between 40° and 60°, depending on the pitch—for both triangular and square cross-sections (see Figure 7a). However, the bending moment necessary to reach this bending (and, thus, the reaction in the clamp) was quite different, given the difference in stiffness between the cross-section shapes (Figure 7b). This implies greater reaction forces (close to double) in the root canal with the square cross-section than with the triangular cross-section, for comparable bending deformations. The effect of the pitch on bending strength was only significant for pitches below 3 mm, where a progressive reduction in strain was observed when the pitch decreased (Figure 9a). This allows for bending of the file to a greater deformation before failure for small pitches, with a corresponding higher expected fatigue life for the same bending deformation (Figure 9b). This effect was especially observed for the triangular cross-section and, to a lesser extent, for the square cross-section. The analysis carried out to estimate the fatigue life also showed that, for the same pitch, the triangular cross-section had a higher expected life than the square cross-section, in agreement with [36], the difference being remarkable for

the smallest pitch analyzed (1 mm), for which the expected life may be more than three times longer.

Our results showed that the orientation of the bending moment, with respect to the cross-section, had a significant effect on the results, changing the results by up to 19.1° and 0.97 N · mm for the square cross-section and up to 13.0° and 0.27 N · mm for the triangular cross-section. This should be taken into account when designing, reporting, and interpreting experimental bending tests according to ISO 3630.

On the other hand, for torsion, the triangular cross-section files could be rotated to a higher angle before failure than those with a square cross-section, as can be observed from Figure 12. However, due to the difference in stiffness, this failure was reached for a torque less than half that for the square cross-section. The effect of the pitch was opposite to that observed in bending, with a reduction in the pitch leading to a lower strength, as shown by the lower possible rotation before failure, which was also in agreement with the results in [36].

From a clinical perspective, the results obtained in this study suggest that the use of a triangular-shaped cross-section with small pitch for endodontic files could be better for the safe shaping of curved root canals, as its lower stiffness would produce less reaction forces in the channel, thus reducing the possibility of ledging and canal transportation. At the same time, files with a triangular cross-section and 1 mm pitch could exhibit a fatigue life more than double that of files with higher pitches or with a square cross-section. This is accompanied by a lower rotational stiffness, which could be beneficial for improving cutting efficiency [36]. The use of a smaller pitch can only partially compensate for this lower torsional stiffness of the triangular cross-section.

The results obtained in this simulation study refer to the boundary conditions established for the tests described in ISO 3630; however, it should be noted that the stress distribution within the file in these tests is not always comparable to the clinical situation, as the bending of the file is also constrained by contact with the canal walls, resulting in a different deformation, depending on the root curvature. As shown in [38], in a curved canal, the maximum strain is usually located near the highest curvature of the curved root canal axis and the fatigue life is clearly dependent on the radius of curvature. Under the conditions of ISO 3630, the highest curvature of the deformed file is close to the tip, so the conclusions in this study are especially valid for root canals with the highest curvature located near the apical end.

Finally, this work has certain limitations that deserve to be mentioned. This investigation was conducted through theoretical studies, by means of finite element analyses of endodontic rotary files; as such, no experimental tests were conducted. Regarding the investigated endodontic file geometries, all of them had uniform parameters (pitch and cross-section) throughout their entire length, even though there exist endodontic instruments in which these parameters vary through their active length. Finally, the bending fatigue life of the endodontic instruments was assessed considering a fully reversed fatigue phenomenon corresponding to a continuous rotation motion of the file within the root canal. The study of the bending fatigue under other types of motion (e.g., reciprocating and adaptive motions) is left for future research.

5. Conclusions

In this study, we simulated the mechanical response of NiTi rotary endodontic files with different cross-sections and pitches using an accurate finite element model under bending and torsion according to the conditions of the ISO 3630 Standard.

From the results obtained, we can conclude that, with equivalent shaft diameter and taper, endodontic files with a square-shaped cross-section have more than double the stiffness of those with a triangular-shaped cross-section under both bending and torsion. The effect of the pitch on stiffness was less significant, but the use of a pitch lower than 3 mm made the files more flexible for bending and stiffer for torsion when using a triangular cross-section, with beneficial effects seen in clinical use. The phase transformation from

austenite to martensite led to a significant decrease in file stiffness both in bending and torsion, which was noticeable in the moment versus deformation curve. When the files were deformed under bending or torsion up to failure, a higher angle of rotation was possible before failure for the triangular section, especially in torsion and, for small pitches, in bending. A higher fatigue life can be expected in clinical use with the triangular-shaped cross-section than for the square cross-section under equivalent file deformations, especially with small pitch values. These results suggest a clinical recommendation for the use of files with triangular-shaped cross-sections and small pitch, in order to minimize ledging and maximize fatigue life.

Under the conditions of the ISO 3630 standard, the orientation of the bending plane with respect to the cross-section of the file had a significant effect on the stiffness and the strength of the file. This effect should be taken into account when designing, reporting, and interpreting similar test results.

Further works on this topic could be focused on studying the mechanical response of endodontic instruments with variable parameters (e.g., in terms of pitch and cross-section) throughout their active length. The bending fatigue life of the endodontic files in cases where the loading conditions do not represent a fully reversed fatigue phenomenon (e.g., adaptive or reciprocating motions) also deserves attention in future investigations.

Author Contributions: Conceptualization, A.P.-G. and V.R.-C.; methodology, A.P.-G. and V.R.-C.; software, V.R.-C.; investigation, A.P.-G. and V.R.-C.; resources, A.Z.-M. and V.F.-M.; writing—original draft preparation, A.P.-G.; writing—review and editing, V.R.-C.; supervision, A.Z.-M. and V.F.-M.; project administration, A.Z.-M. and V.F.-M. All authors have read and agreed to the published version of the manuscript.

Funding: This research received no external funding.

Institutional Review Board Statement: Not applicable.

Informed Consent Statement: Not applicable.

Data Availability Statement: Not applicable.

Conflicts of Interest: The authors declare no conflicts of interest.

Appendix A. Post-Processing of the Finite Element Analysis Results

Appendix A.1. Assessment of the Maximum von Mises Stress and Maximum Principal Strain Values in the Endodontic File

Due to the nature of the finite element method, stress and strain singularities may appear in the vicinity of those regions of the model where boundary conditions are applied or in those areas nearby geometric stress increases. These singularities imply that unrealistically large values of stress–strain are obtained as a consequence of the numerical treatment used to derive these magnitudes from the nodal displacement results. There are many researchers who have claimed that the stress–strain results at singularity points cannot be considered when evaluating the strength of endodontic files [41,42].

Several strategies can be found in the literature to address this issue. Żmudzki [43] proposed to exclude the stress results at these points, instead extrapolating the extreme value from the stress values in the surrounding nodes. A different approach has been used by Baek [36], who determined the maximum stress level as the mean value of the top 1% von Mises equivalent stress values in the finite element model. In this work, the maximum von Mises stress σ_{max} at a given analysis frame is defined as the maximum stress level that is reached by a certain amount λ of the total volume of the file (V_{tot}). To determine this magnitude, the steps below were followed:

- Let $i \in [1, n_e]$ refer to each of the n_e tetrahedral finite elements in the model, and $j \in [1, 4]$ refer to the integration points in each tetrahedral element. The von Mises stress at a given element and integration point is denoted as σ_{ij}, and the volume

associated with each integration point is denoted as $V_{ij} = V_i/4$ (where V_i is the volume of element i).

- The von Mises stress σ_{ij} and the volume V_{ij} at each integration point of the model are retrieved and stored in an array Σ with $n_i = 4 \cdot n_e$ rows. Each row m in Σ contains the von Mises stress and the volume associated with a given integration point, with the shape

$$\Sigma[m] = [\sigma_{ij}, V_{ij}]. \quad \text{(A1)}$$

- The rows in Σ are rearranged in such a way that the von Mises stresses are sorted in descending order. Then, the algorithm shown in Figure A1 is applied to determine the maximum von Mises stress in the analysis frame.

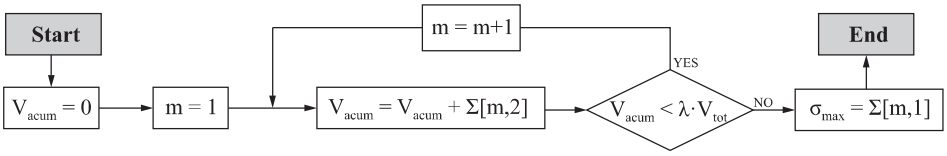

Figure A1. Algorithm to search for the maximum von Mises σ_{ij} stress in the analysis frame after the array Σ is created.

In this work, the magnitude of λ is set arbitrarily to 0.1‰, which has been shown to be a good value to avoid stress singularities while maintaining the actual stress level of the file. The same strategy was applied to determine the maximum principal strain in each analysis frame.

Appendix A.2. Determination of Bending Fatigue Life of the NiTi Endodontic Files

When the endodontic files are continuously rotated inside the root canal, they are typically subjected to a purely reversed fatigue phenomenon in which, for each rotation of the file, the bending strain alternates between nearly equal positive and negative peak values following a sinusoidal function [44]. The difference between these peak values is called the bending strain range, which is denoted by $\Delta\varepsilon$. Several studies [45–47] have demonstrated that the bending strain range and the number of cycles to failure (NCF) are correlated, and this correlation can be adequately represented by the Coffin–Manson relation:

$$\frac{\Delta\varepsilon}{2} = \varepsilon'_F \cdot N_f^c + \frac{\sigma'_F}{E} \cdot N_f^b, \quad \text{(A2)}$$

where N_f is equivalent to the NCF, ε'_F is the fatigue ductility coefficient, σ'_F is the fatigue strength coefficient, c is the fatigue ductility exponent, and b is the fatigue strength exponent.

Two issues arise when applying the Coffin–Manson relation to predict the NCF of the endodontic files from the strain results obtained from the proposed finite element model:

- On one hand, the Coffin–Manson relation is based on a uni-axial strain, but the strain results obtained from the finite element model correspond to a multi-axial strain state. Thus, a criterion to reduce the obtained multi-axial strain state to an equivalent uni-axial strain condition is required.
- On the other hand, the bending analysis conducted using the proposed finite element model does not represent the actual strain history of the endodontic file when it is rotating inside the root canal, as bending is applied in just one direction (uni-directional fatigue). Thus, a conversion method must be proposed to convert the obtained strains into a purely reversed fatigue phenomenon.

According to Roda-Casanova et al. [44], and in order to convert the multi-axial strain state into uni-axial strain, the bending strain range $\Delta\varepsilon_i$ at node i of the finite element model can be successfully approximated by:

$$\Delta\varepsilon_i = \max_{j=1\ldots n_f} (\varepsilon_{ij}^{max}) - \min_{j=1\ldots n_f} (\varepsilon_{ij}^{min}), \tag{A3}$$

where ε_{ij}^{max} and ε_{ij}^{min} are the maximum and the minimum principal strains that take place at node i at time frame j of the transient analysis, respectively. Considering that the endodontic file is continuously rotating inside the root canal, it is fair to assume that the maximum and minimum principal strains that take place at node i have the same modulus and different sign. Under this assumption, Equation (A3) can be simplified to:

$$\Delta\varepsilon_i = 2 \cdot \max_{j=1\ldots n_f} (\varepsilon_{ij}^{max}). \tag{A4}$$

Thus, by determining the maximum magnitude of the maximum principal strain in the finite element model and calculating the strain range $\Delta\varepsilon_i$ at such a node using Equation (A4), the NCF for a given specimen can be predicted through Equation (A2). The material parameters considered for the application of the Coffin–Manson relation are reflected in Table 2.

Appendix B. Literature Review

Table A1. Previous FE studies considering the effects of cross-section and pitch on rotary endodontic files.

Source	Section Type	Tip Diameter; Taper	Pitch (mm)	Material Model and Parameters	FE Code; Model Type	Boundary Conditions; Number of Nodes/Elements	Conclusions	Limitations
Xu et al., 2006 [32]	6 shapes (ProTaper, Hero642, Mtwo, ProFile, Quantec, NiTiflex)	0.4 mm, 4%	3.6	Multi-linear kinematic hardening plastic model E_A = 34.3 GPa, ν_A = 0.33, σ_L^S = 480 MPa, σ_L^F = 755 MPa	N/A, Static	Loads: progressive 0–2.5 Nmm torsion in shank, Constraints: fixed at tip, # nodes: Not available. # elements: Not available.	(1) Sections with higher core area show lower stresses for the same torque	(1) Sections analyzed have different total areas
Kim et al., 2009 [34]	4 shapes (ProFile, HeroShaper, Mtwo, NRT)	0.3 mm; 6%	Several, N/A	E_A = 36 GPa, ν_A = 0.3, σ_L^F = 504 MPa, σ_L^S = 755 MPa	ABAQUS; Static (cases I to IV) Dynamic (case V): Simulated shaping	Case I (or II), Load: 1 N (or 2 mm) bending in tip Constraint: shank fixed Case II (or III), Load: 2.5 Nmm (or 10°) torsion in shank Constraint: fixed at 4 mm from tip Case V, Constraint: shank rotation 240 rpm, file introduction in simulated root canal; # nodes: 7018–18,214 # elements: 5300–9440	(1) Rectangle-based sections have lower expected fatigue life than triangle-based sections	(1) Material model not clearly defined
Baek et al., 2011 [36]	4 theoretical shapes (triangle, slender rectangle, rectangle, square)	0.3 mm; 4.4%	3.2, 1.6, 1.1	E_A = 36 GPa, ν_A = 0.3	ABAQUS; Static	Load: 20° torsion in shank Constraint: fixed at 4 mm from tip; # nodes: Not available. # elements: Not available.	(1) Rectangle-based sections, even with smaller areas, have higher torsional stiffness than triangular section; (2) Reduction in pitch increases torsional stiffness	(1) Linear material model; (2) Mesh quality not provided
Arbab-Chirani et al., 2011 [35]	5 shapes (Hero, Hero Shaper, Mtwo, ProFile, ProTaper F1)	0.2mm; 6%	Several, N/A	SMA material model, E_A = 47 GPa, ν_A = 0.3 σ_L^S = 505 MPa	Cast3M; Static	Case 1: Load: bending at tip 3.8 mm, Constraint: shank fixed Case 2: Load: torsion at tip 22°, Constraint: shank fixed; # nodes: 66,023–73,561 # elements: 14,100–16,200	(1) ProTaper F1, Hero Shaper, and Hero are stiffer than Mtwo and ProFile; (2) Maximum stresses near the tip for both cases and similar for all the files	(1) Different pitch among files; (2) Deformations applied are low to extend martensitic transformation to a significant part of the file

Table A1. *Cont.*

Source	Section Type	Tip Diameter; Taper	Pitch (mm)	Material Model and Parameters	FE Code; Model Type	Boundary Conditions; Number of Nodes/Elements	Conclusions	Limitations
Versluis et al., 2012 [33]	4 theoretical shapes (triangle, slender rectangle, rectangle, square)	0.3 mm; 4%	3.2, 1.6, 1.1	SMA material model, E_A = 36 GPa, ν_A = 0.3 σ_L^S = 504 MPa, σ_L^E = 600 MPa	MSC.Marc; Static	Load: bending at tip 5 mm (all possible orientations with respect to the cross-section), Constraint: shank axis orientation and shank end location fixed; # nodes: Not available. # elements: Not available.	(1) Flexural stiffness and stress decreases with decreasing pitch; (2) Decreasing the pitch reduces the oscillation of stress when the file rotates; (3) Flexural stiffness and stress correlates with center-core area; (4) Effect of section greater than that of pitch; (5) Maximum stress is affected by bending orientation for rectangular section	(1) Deformations applied are low to extend martensitic transformation to a significant part of the file (max. stresses below 504 MPa)
De Arruda et al., 2014 [10]	3 shapes (Mtwo, RaCe, PTU F1)	0.25 mm; 6%	Several (Not available)	Shape-memory alloy material model implemented as ABAQUS sub-routine, E_A = 42.53 GPa, ν_A = 0.33 σ_L^S = 492 MPa, σ_L^E = 630 MPa	ABAQUS; Static	Case 1: Load: bending in shank from 0º to 45º (two perpendicular orientations), Constraint: fixed at 3 mm from tip Case 2: Load: 3 Nmm torsion in shank, Constraint: fixed at 3 mm from tip; # nodes: 84,126–91,372 # elements: 48,460–55,009	(1) Finite element analysis results agree with experimental results; (2) RaCe and Mtwo are more flexible than PTU F1 in bending and torsion; (3) Shape of the section affects the maximum stress and the variation in stress with bending orientation	(1) Only three section geometries and two orientations for bending considered; (2) Different pitch among files
Ha et al., 2015 [37]	4 theoretical shapes (triangle, slender rectangle, rectangle, square)	0.3 mm; 4.4%	3.2, 1.6, 1.1	E_A = 26 GPa, ν_A = 0.3	ABAQUS; Not available.	Load: Prescribed rotation inside the root canal, Constraint: Contact with friction in 3 simulated root canal (15º, 30º, 45º curvature), shank axis orientation & shank end location fixed; # nodes: 10,230–18,042 # elements: 8325–15,540	(1) The square cross-section shows the highest 'screw-in' force and reaction torque; (2) 'Screw-in' force and reaction torque are higher for greater pitch and higher root canal curvature	(1) Linear material model; (2) Very low friction coefficient (0.1) considered between file and root canal; (3) Solid surface used as root canal model; (4) Only 3 root canal geometries considered
Basser-Ahamed et al., 2018 [31]	5 theoretical shapes (triangle T, convex triangle C, concave triangle U, combined CTU, combinedUTC)	0.25 mm; 6%	1.6	File: E_A = 36 GPa, ν_A = 0.3 Root canal: E = 18.6 GPa, ν_A = 0.3	ANSYS; Not available.	Load: Torque 2 Nm, Constraint: Contact with simulated root canal (45º curvature), shank axis orientation and shank end location fixed, rotation of 180º at 240 rpm; File: # nodes: 16,750–42,785 # elements: 75,430–152,432 Root canal: # nodes: 3000 # elements: 3500	(1) A combined section CTU (C coronal third, T middle third, U apical third) presents lower stresses than constant section	(1) Geometry of the root canal not clearly defined defined; (2) Contact and friction conditions undefined; (3) Does not consider changes in dentin properties within the root canal; (4) Effect of pitch not analyzed

References

1. Walia, H.; Brantley, W.; Gerstein, H. An initial investigation of the bending and torsional properties of nitinol root canal files. *J. Endod.* **1988**, *14*, 346–351. https://doi.org/10.1016/S0099-2399(88)80196-1.
2. Esposito, P.; Cunningham, C. A comparison of canal preparation with nickel-titanium and stainless steel instruments. *J. Endod.* **1995**, *21*, 173–176. https://doi.org/10.1016/S0099-2399(06)80560-1.
3. Bergmans, L.; Van Cleynenbreugel, J.; Wevers, M.; Lambrechts, P. Mechanical root canal preparation with NiTi rotary instruments: Rationale, performance and safety. Status Report for the American Journal of Dentistry. *Am. J. Dent.* **2001**, *14*, 324–333.
4. Parashos, P.; Gordon, I.; Messer, H. Factors influencing defects of rotary nickel-titanium endodontic instruments after clinical use. *J. Endod.* **2004**, *30*, 722–725. https://doi.org/10.1097/01.DON.0000129963.42882.C9.
5. Spili, P.; Parashos, P.; Messer, H. The impact of instrument fracture on outcome of endodontic treatment. *J. Endod.* **2005**, *31*, 845–850. https://doi.org/10.1097/01.don.0000164127.62864.7c.
6. Plotino, G.; Grande, N.M.; Cordaro, M.; Testarelli, L.; Gambarini, G. A Review of Cyclic Fatigue Testing of Nickel-Titanium Rotary Instruments. *J. Endod.* **2009**, *35*, 1469–1476. https://doi.org/10.1016/j.joen.2009.06.015.
7. Scattina, A.; Alovisi, M.; Paolino, D.S.; Pasqualini, D.; Scotti, N.; Chiandussi, G.; Berutti, E. Prediction of cyclic fatigue life of nickel-titanium rotary files by virtual modeling and finite elements analysis. *J. Endod.* **2015**, *41*, 1867–1870. https://doi.org/10.1016/j.joen.2015.07.010.
8. Peters, O.; Barbakow, F. Dynamic torque and apical forces of ProFile .04 rotary instruments during preparation of curved canals. *Int. Endod. J.* **2002**, *35*, 379–389. https://doi.org/10.1046/j.0143-2885.2001.00494.x.
9. Kuhn, G.; Tavernier, B.; Jordan, L. Influence of structure on nickel-titanium endodontic instruments failure. *J. Endod.* **2001**, *27*, 516–520. https://doi.org/10.1097/00004770-200108000-00005.
10. De Arruda Santos, L.; López, J.; De Las Casas, E.; De Azevedo Bahia, M.; Buono, V. Mechanical behavior of three nickel-titanium rotary files: A comparison of numerical simulation with bending and torsion tests. *Mater. Sci. Eng. C* **2014**, *37*, 258–263. https://doi.org/10.1016/j.msec.2014.01.025.
11. Pruett, J.; Clement, D.; Carnes, D., Jr. Cyclic fatigue testing of nickel-titanium endodontic instruments. *J. Endod.* **1997**, *23*, 77–85. https://doi.org/10.1016/S0099-2399(97)80250-6.
12. Parashos, P.; Messer, H. Rotary NiTi Instrument Fracture and its Consequences. *J. Endod.* **2006**, *32*, 1031–1043. https://doi.org/10.1016/j.joen.2006.06.008.
13. Topçuoğlu, H.; Topçuoğlu, G. Cyclic Fatigue Resistance of Reciproc Blue and Reciproc Files in an S-shaped Canal. *J. Endod.* **2017**, *43*, 1679–1682. https://doi.org/10.1016/j.joen.2017.04.009.
14. Siqueira, J., Jr.; Rôças, I. Polymerase chain reaction-based analysis of microorganisms associated with failed endodontic treatment. *Oral Surgery Oral Med. Oral Pathol. Oral Radiol. Endod.* **2004**, *97*, 85–94. https://doi.org/10.1016/S1079-2104(03)00353-6.
15. Strindberg, L. The Dependence of the Results of Pulp Therapy on Certain Factors: An Analytic Study Based on Radiographic and Clinical Follow-Up Examinations. *Acta Odontol Scand* **1956**, *14*, 1–175.
16. Yang, Q.; Shen, Y.; Huang, D.; Zhou, X.; Gao, Y.; Haapasalo, M. Evaluation of Two Trephine Techniques for Removal of Fractured Rotary Nickel-titanium Instruments from Root Canals. *J. Endod.* **2017**, *43*, 116–120. https://doi.org/10.1016/j.joen.2016.09.001.
17. Fu, M.; Zhang, Z.; Hou, B. Removal of broken files from root canals by using ultrasonic techniques combined with dental microscope: A retrospective analysis of treatment outcome. *J. Endod.* **2011**, *37*, 619–622. https://doi.org/10.1016/j.joen.2011.02.016.
18. Ruiz-Sánchez, C.; Faus-Llacer, V.; Faus-Matoses, I.; Zubizarreta-Macho, A.; Sauro, S.; Faus-Matoses, V. The influence of niti alloy on the cyclic fatigue resistance of endodontic files. *J. Clin. Med.* **2020**, *9*, 3755. https://doi.org/10.3390/jcm9113755.
19. Zupanc, J.; Vahdat-Pajouh, N.; Schäfer, E. New thermomechanically treated NiTi alloys—A review. *Int. Endod. J.* **2018**, *51*, 1088–1103. https://doi.org/10.1111/iej.12924.
20. Faus-Llacer, V.; Kharrat, N.; Ruiz-Sanchez, C.; Faus-Matoses, I.; Zubizarreta-Macho, A.; Faus-Matoses, V. The effect of taper and apical diameter on the cyclic fatigue resistance of rotary endodontic files using an experimental electronic device. *Appl. Sci.* **2021**, *11*, 863. https://doi.org/10.3390/app11020863.
21. Turpin, Y.; Chagneau, F.; Vulcain, J. Impact of two theoretical cross-sections on torsional and bending stresses of nickel-titanium root canal instrument models. *J. Endod.* **2000**, *26*, 414–417. https://doi.org/10.1097/00004770-200007000-00009.
22. Sekar, V.; Kumar, R.; Nandini, S.; Ballal, S.; Velmurugan, N. Assessment of the role of cross section on fatigue resistance of rotary files when used in reciprocation. *Eur. J. Dent.* **2016**, *10*, 541–545. https://doi.org/10.4103/1305-7456.195171.
23. Kwak, S.; Ha, J.H.; Lee, C.J.; El Abed, R.; Abu-Tahun, I.; Kim, H.C. Effects of Pitch Length and Heat Treatment on the Mechanical Properties of the Glide Path Preparation Instruments. *J. Endod.* **2016**, *42*, 788–792. https://doi.org/10.1016/j.joen.2016.02.002.
24. *ISO 3630-1:2008*; Dentistry—Root-Canal Instruments—Part 1: General Requirements and Test Methods. International Organization for Standardization: Geneva, Switzerland, 2008.
25. Zhang, E.; Cheung, G.; Zheng, Y. A mathematical model for describing the mechanical behaviour of root canal instruments. *Int. Endod. J.* **2011**, *44*, 72–76. https://doi.org/10.1111/j.1365-2591.2010.01801.x.
26. Tsao, C.; Liou, J.; Wen, P.; Peng, C.; Liu, T. Study on bending behaviour of nickel-titanium rotary endodontic instruments by analytical and numerical analyses. *Int. Endod. J.* **2013**, *46*, 379–388. https://doi.org/10.1111/iej.12025.
27. Lee, M.H.; Versluis, A.; Kim, B.M.; Lee, C.J.; Hur, B.; Kim, H.C. Correlation between experimental cyclic fatigue resistance and numerical stress analysis for nickel-titanium rotary files. *J. Endod.* **2011**, *37*, 1152–1157. https://doi.org/10.1016/j.joen.2011.03.025.

28. Montalvão, D.; Shengwen, Q.; Freitas, M. A study on the influence of Ni-Ti M-Wire in the flexural fatigue life of endodontic rotary files by using Finite Element Analysis. *Mater. Sci. Eng. C* **2014**, *40*, 172–179. https://doi.org/10.1016/j.msec.2014.03.061.
29. Bonessio, N.; Pereira, E.; Lomiento, G.; Arias, A.; Bahia, M.; Buono, V.; Peters, O. Validated finite element analyses of WaveOne Endodontic Instruments: A comparison between M-Wire and NiTi alloys. *Int. Endod. J.* **2015**, *48*, 441–450. https://doi.org/10.1111/iej.12333.
30. Chien, P.Y.; Walsh, L.J.; Peters, O.A. Finite element analysis of rotary nickel-titanium endodontic instruments: A critical review of the methodology. *Eur. J. Oral Sci.* **2021**, *129*, e12802. https://doi.org/10.1111/eos.12802.
31. Basheer Ahamed, S.; Vanajassun, P.; Rajkumar, K.; Mahalaxmi, S. Comparative Evaluation of Stress Distribution in Experimentally Designed Nickel-titanium Rotary Files with Varying Cross Sections: A Finite Element Analysis. *J. Endod.* **2018**, *44*, 654–658. https://doi.org/10.1016/j.joen.2017.12.013.
32. Xu, X.; Eng, M.; Zheng, Y.; Eng, D. Comparative study of torsional and bending properties for six models of nickel-titanium root canal instruments with different cross-sections. *J. Endod.* **2006**, *32*, 372–375. https://doi.org/10.1016/j.joen.2005.08.012.
33. Versluis, A.; Kim, H.C.; Lee, W.; Kim, B.M.; Lee, C.J. Flexural stiffness and stresses in nickel-titanium rotary files for various pitch and cross-sectional geometries. *J. Endod.* **2012**, *38*, 1399–1403. https://doi.org/10.1016/j.joen.2012.06.008.
34. Kim, H.; Kim, H.; Lee, C.; Kim, B.; Park, J.; Versluis, A. Mechanical response of nickel-titanium instruments with different cross-sectional designs during shaping of simulated curved canals. *Int. Endod. J.* **2009**, *42*, 593–602. https://doi.org/10.1111/j.1365-2591.2009.01553.x.
35. Arbab-Chirani, R.; Chevalier, V.; Arbab-Chirani, S.; Calloch, S. Comparative analysis of torsional and bending behavior through finite-element models of 5 Ni-Ti endodontic instruments. *Oral Surgery Oral Med. Oral Pathol. Oral Radiol. Endodontology* **2011**, *111*, 115–121. https://doi.org/10.1016/j.tripleo.2010.07.017.
36. Baek, S.H.; Lee, C.J.; Versluis, A.; Kim, B.M.; Lee, W.; Kim, H.C. Comparison of torsional stiffness of nickel-titanium rotary files with different geometric characteristics. *J. Endod.* **2011**, *37*, 1283–1286. https://doi.org/10.1016/j.joen.2011.05.032.
37. Ha, J.H.; Cheung, G.S.; Versluis, A.; Lee, C.J.; Kwak, S.W.; Kim, H.C. 'Screw-in' tendency of rotary nickel-titanium files due to design geometry. *Int. Endod. J.* **2015**, *48*, 666–672. https://doi.org/10.1111/iej.12363.
38. Roda-Casanova, V.; Zubizarreta-Macho, A.; Sanchez-Marin, F.; Ezpeleta, O.; Martínez, A.; Catalán, A. Computerized generation and finite element stress analysis of endodontic rotary files. *Appl. Sci.* **2021**, *11*, 4329. https://doi.org/10.3390/app11104329.
39. Auricchio, F.; Petrini, L. A three-dimensional model describing stress-temperature induced solid phase transformations: Solution algorithm and boundary value problems. *Int. J. Numer. Methods Eng.* **2004**, *61*, 807–836. https://doi.org/10.1002/nme.1086.
40. El-Anwar, M.I.; Mandorah, A.O.; Yousief, S.A.; Soliman, T.A.; Abd El-Wahab, T.M. A finite element study on the mechanical behavior of reciprocating endodontic files. *Braz. J. Oral Sci.* **2015**, *14*, 52–59. https://doi.org/10.1590/1677-3225v14n1a11.
41. Stolk, J.; Verdonschot, N.; Huiskes, R. Management of stress fields around singular points in a finite element analysis. *Comput. Methods Biomech. Biomed. Eng.* **2001**, *3*, 57–62.
42. Chen, G.; Pettet, G.; Pearcy, M.; McElwain, D. Comparison of two numerical approaches for bone remodelling. *Med. Eng. Phys.* **2007**, *29*, 134–139. https://doi.org/https://doi.org/10.1016/j.medengphy.2005.12.008.
43. Żmudzki, J.; Chladek, W. Stress present in bone surrounding dental implants in FEM model experiments. *J. Achiev. Mater. Manuf. Eng.* **2008**, *27*, 71–74.
44. Roda-Casanova, V.; Pérez-González, A.; Zubizarreta-Macho, Á.; Faus-Matoses, V. Fatigue Analysis of NiTi Rotary Endodontic Files through Finite Element Simulation: Effect of Root Canal Geometry on Fatigue Life. *J. Clin. Med.* **2021**, *10*, 5692. https://doi.org/10.3390/jcm10235692.
45. Cheung, G.S.; Darvell, B.W. Fatigue testing of a NiTi rotary instrument. Part 1: Strain-life relationship. *Int. Endod. J.* **2007**, *40*, 612–618. https://doi.org/10.1111/j.1365-2591.2007.01262.x.
46. Figueiredo, A.M.; Modenesi, P.; Buono, V. Low-cycle fatigue life of superelastic NiTi wires. *Int. J. Fatigue* **2009**, *31*, 751–758. https://doi.org/10.1016/j.ijfatigue.2008.03.014.
47. Maletta, C.; Sgambitterra, E.; Furgiuele, F.; Casati, R.; Tuissi, A. Fatigue properties of a pseudoelastic NiTi alloy: Strain ratcheting and hysteresis under cyclic tensile loading. *Int. J. Fatigue* **2014**, *66*, 78–85. https://doi.org/10.1016/j.ijfatigue.2014.03.011.